Project Title:

Theoretical study of interaction between tunneling electrons and individual molecules at surfaces

Name:○Yousoo Kim, Emi Minamitani, Jaehoon Jung, Seiji Takemoto, Hiroshi Imada*, Miyabi Imai*, Taketoshi Minato*, Ju-Hyung Kim*

**During FY2012, two users of our group, T. Minato and J.-H. Kim, were changed to H. Imada and M. Imai.*

Laboratory: Surface and Interface Science Laboratory, RIKEN Advanced Science Institute, RIKEN Wako Institute

（和光研究所 基幹研究所 Kim 表面界面科学研究室）

---

1. Background and purpose of the project, relationship of the project with other projects.

During the past decade, computer simulations based on a quantum mechanics have developed an increasingly important impact on solid-state physics and chemistry and on materials science. In field of material science, the surface chemistry is fundamentally important in many areas, such as molecular electronics, heterogeneous catalyst, fuel cell, etc. The adsorption of molecules onto a surface is a necessary prerequisite to any surface mediated chemical process. Understanding the bonding nature between the molecule and the surface on the basis of the electronic structure is therefore one of the most important issues in this field. The computational methods like density functional theory (DFT) have played a prominent role to elucidate the interaction between the molecule and the surface.

From the theoretical investigation of the adsorbed molecule on surface in combination with scanning tunneling microscopy and spectroscopy (STM/STS) experiment, we could expect the following research goals; 1) the deep understanding of the chemical/physical properties of an adsorbate on the surface, 2) the fine control of the chemistry on the surface.

2. Specific usage status of the system and calculation method

We have been studying the molecular adsorption on the well-defined metal surface using computational method in combination with experimental method. In our studies, first-principles simulations have been carried out using the Vienna Ab-initio Simulation Package (VASP) code in the density functional level of theory. The pure DFT methods have been mostly used and the inner electrons are replaced by projector augmented wave pseudopotentials (PAW). The climbing image nudged elastic band method (CI-NEB) was used to determine the transition states which were confirmed by imaginary frequency modes. In most of cases, STM image simulations were performed using Tersoff-Hamann approach. The computational results have been compared with the available experimental result obtained from STM in our group.

We also have been studying the many-body phenomena in molecular adsorption system, in particular the Kondo effect. The characteristic electronic state resulting from the Kondo effect, so-called Kondo singlet state appears as a sharp peak structure (Kondo peak) at the Fermi level in STS. In order to simulate the Kondo peak, we build numerical renormalization group (NRG) code and the STS simulation code based on the Keldysh Green's function method.

3. Results

(1) Ligand field effect at oxide-metal interface on the chemical reactivity of ultrathin oxide film surface

Ultrathin oxide films grown on metal substrate are of great interest not only as supporting materials for chemically active nanoparticles but also as catalysts in the field of heterogeneous catalysis [H.-J. Freund, *Chem. Eur. J.* **16**, 9384 (2010)]. Using STM and DFT calculations, we have demonstrated that the chemical reactivity for water dissociation on an ultrathin MgO film grown on Ag(100) substrate depends greatly on film thickness and is enhanced as compared to that achieved with their bulk counterpart [H.-J. Shin et al., *Nature Mater.* **9**, 442 (2010); J. Jung et al., *Phys. Rev. B* **82**, 085413 (2010)]. The change of chemical reactivity of ultrathin MgO film depending on the film thickness can be explained by the strengthening of the interaction between the oxide and metal interface layers. This result implies that the artificial manipulation of the local structure at the oxide-metal interface is expected to play a pivotal role in controlling the catalytic activity of oxide film. As a preliminary study, we also reported that water dissociation on three model systems with defects at the oxide-metal interface of the 2-ML MgO/Ag(100) - an O vacancy, an Mg impurity, or an O impurity - can improve the chemical reactivity of ultrathin MgO film supported by Ag(100) substrate using periodic DFT calculations [J. Jung et al., *J. Am. Chem. Soc.* **133**, 6142 (2011)].

Based on our previous results, we performed the systematic computational study on controlling the chemical reactivity of ultrathin MgO film grown on Ag(100) substrate for the dissociation of individual water molecules by 3d transition metal (TM) interface dopants (Fig. 1) [J. Jung et al., *J. Am. Chem. Soc.* **134**, 10554 (2012)].

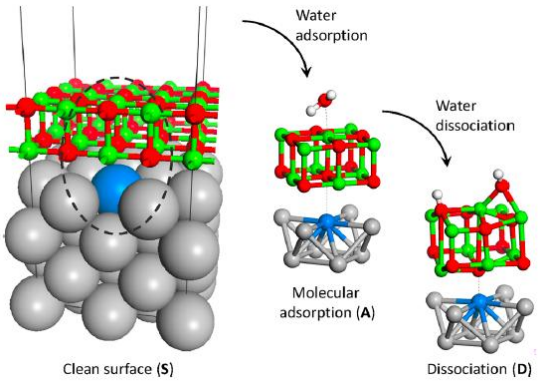

Figure 1. Dissociation of water molecules on ultrathin MgO film grown on Ag(100) substrate with interface dopants of first row 3d transition metal (TM). (Ag, gray; 3d TM dopant, blue; Mg, green; O, red; H, white).

To investigate the influence of interface dopant on the chemical reactivity of ultrathin oxide film for the dissociation of water molecules, we examined the dissociation mechanism of individual water molecules adsorbed upon a MgO film surface with a dopant as shown in Fig. 2a. A water molecule first adsorbs asymmetrically on top of the surface magnesium (Mg1), located over a transition metal (TM) dopant (D_{TM}), where one hydrogen atom (H1) interacts with a neighboring surface oxygen (O_s) via hydrogen bonding. When the water molecule dissociates into $H^+ + OH^-$, H^+ forms a hydroxyl ion (O_sH1) by bonding with surface oxygen, and OH^- (O_wH2) bonds with the two nearest magnesium ions (Mg1 and Mg2). ("w" and "s" denote water and surface, respectively.) It should be noted that the dissociation mechanism is not changed by the interface dopants compared with the non-doped system, which means that the chemical reactivity of the MgO film grown on a Ag(100) substrate can be controlled by interface manipulation with the established mechanism. Figure 2b shows the reaction energy diagram for the dissociation of individual water molecules on non-doped (ND) 1- and 2-ML MgO/Ag(100) surfaces and on an MgO film surface deposited on a Ti-doped Ag substrate (*int*-Ti_{dop}), where Ti is the most reactive dopant

among all the 3d TM series (see also Fig. 2c).

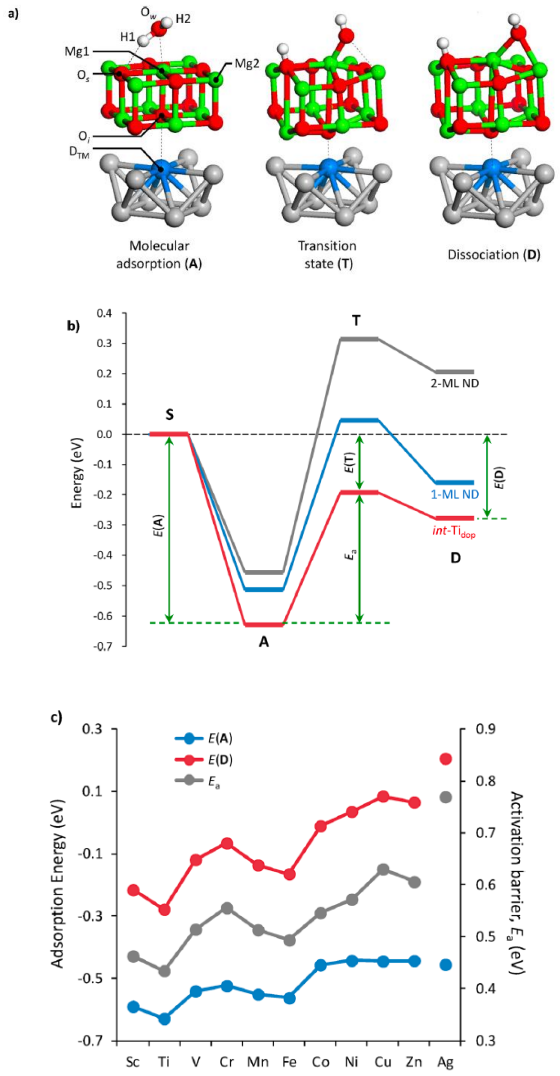

Figure 2. Water dissociation on MgO/Ag(100) with interface dopants. (a) Dissociation mechanism of the individual water molecule on an ultrathin MgO film supported by doped and non-doped Ag(100) substrates. (Ag, grey; 3d TM dopant, blue; Mg, green; O, red; H, white) (b) Reaction energy diagram (in eV) for the water dissociation on the non-doped (ND) 2-ML MgO/Ag(100) surfaces and on MgO film surface deposited on a Ti-doped Ag(100) substrate (*int*-Ti_{dop}) at the oxide-metal interface. Non-dissociative adsorption (**A**), transition state (**T**) and dissociative adsorption (**D**) energies are evaluated relative to $E(H_2O) + E(\text{Substrate}) = 0$ eV. Dissociation barrier, $E_a = E(\mathbf{T}) - E(\mathbf{A})$. (c) The variations of $E(\mathbf{A})$, $E(\mathbf{D})$ and E_a along the 3*d* TM (Sc ~ Zn) dopants.

A remarkable improvement in chemical reactivity for water dissociation over thickness dependence was achieved in *int*-Ti_{dop}, where the water molecule is more strongly adsorbed and more easily dissociated on *int*-Ti_{dop}. The non-dissociative molecular adsorption ($E(\mathbf{A})$), transition state ($E(\mathbf{T})$), and dissociative adsorption ($E(\mathbf{D})$) energies for *int*-Ti_{dop} are lower than those of ND film with same film thickness by 0.17, 0.51, and 0.48 eV, respectively. The barrier height (E_a), $E(\mathbf{T}) - E(\mathbf{A})$, is, therefore, noticeably reduced by 44% and 60% from those of 2-ML ND MgO film and bulk MgO, respectively.

Our systematic study on the doping of 3d TM into the oxide-metal interface provides a new perspective that the chemical reactivity of ultrathin oxide film grown on a metal substrate can be finely tuned by interface manipulation. Figure 2c shows the variation of the reaction energies, such as $E(\mathbf{A})$, $E(\mathbf{D})$ and E_a, during the dissociation of individual water molecules on MgO/Ag(100) according to the kind of interface dopant (Sc ~ Zn). Interestingly, the shape of reaction energy variation along 3d TM series clearly shows a "double-humped pattern" which is commonly observed in organometallic systems explained by ligand field stabilization energy (LFSE) with weak field ligands. The electronic configuration of high-spin TM complexes represented by the small ligand field splitting of TM d orbitals results in a characteristic double-humped pattern according to the amount of d electron stabilization such as the hydration enthalpy of bivalent TM ions ($[TM(H_2O)_6]^{2+}$). Because the only compositional difference among the systems is a TM dopant introduced into the interfacial metal layer, the result illustrated in Fig. 2c reasonably suggests that interfacial D_{TM}–O_i interaction is closely related to the chemical reactivity of ultrathin MgO film.

Although the nature of the interfacial interaction between oxide film and a metal substrate cannot be easily described by a single term, we show that the chemical reactivity of an ultrathin oxide film supported by a doped-metal substrate can be mainly governed by the hybridization between the electronic

states of a D_{TM} and an O_i (of oxide layer) at the interface. For systematic study on the influence of dopants upon the electronic structure at the oxide-metal interface, the projected density of states (PDOS) diagrams of $3d_{z^2}$ (D_{TM}) and $2p_z(O_i)$ states for the all doped MgO/Ag(100) systems are illustrated in Figs 3a and 3b, respectively.

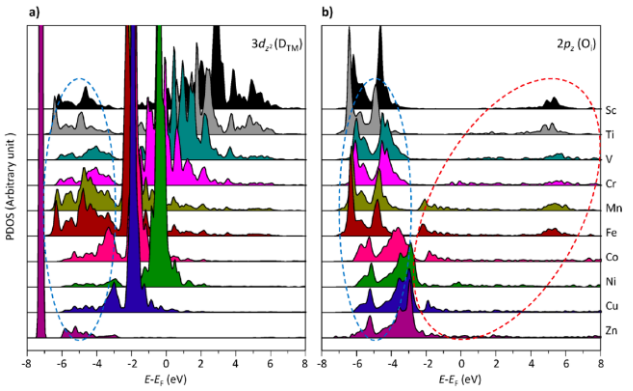

Figure 3. Electronic structure at the interface determined by ligand field effect. Projected density of states (PDOS) of 3d TM (D_{TM}) doped MgO/Ag(100) (*int*-M_{dop}, M = Sc ~ Zn) before the adsorption of water molecule (**S**); (a) $3d_z^2$ (D_{TM}) and (b) $2p_z$ (O_i). The scale in the y-axis is (a):(b) = 2:1. Only up-spin states are plotted for clarity considering the weak field nature. Bonding and anti-bonding states are depicted in (a) and (b) with blue and red dotted lines, respectively.

The distribution of electronic states for bonding and anti-bonding states is depicted by dotted blue and red circles, respectively, on the PDOS diagram of $2p_z(O_i)$ states. The identical alignment of the bonding states (about –7 ~ –3 eV) between a D_{TM} and an O_i in PDOS diagrams indicates the existence of orbital interaction along the z-axis at the interface. Hybridization, i.e., the formation of bonding and anti-bonding states, between the electronic states of D_{TM} and O_i indicates that ultrathin MgO film behaves as a ligand for the interface dopants. The correlation between global adhesion strength and the local D_{TM}–O_i interaction is also well explained by the PDOS diagrams. At the higher 3d series (Mn ~ Zn), the anti-bonding states become partially occupied (about –2 ~ 0 eV, Fig. 3b) and their adhesion energies decrease overall compared to the lower 3d series, as shown in Fig. 4.

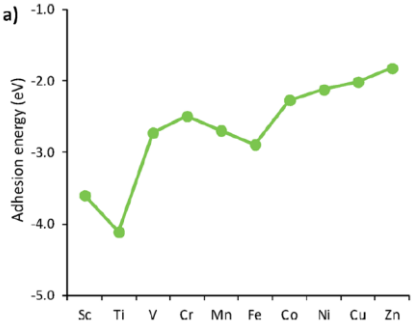

Figure 4. Double-humped pattern in the adhesion energy of the interface doped MgO/Ag(100). The variations of adhesion energy between oxide and metal layers, $E_{adh} = E(int\text{-}M_{dop}) - [E(\text{MgO}) + E(M\text{-doped Ag})]$, are calculated using the corresponding geometry in the optimized structure for **S** stage.

Our results revealed that the chemical reactivity of the oxide film surface is strongly dependent on the tailored electronic structure caused by the interface dopants at the impurity level, which implies that chemical reactivity can be systematically controlled by adjusting adhesion strength using interface dopants. This observation strongly suggests the advantage of interface manipulation compared to direct modification of a surface structure. The manipulated interface can be protected from chemical reactions by ultrathin oxide film. Therefore, the durability of the developed system and the fine-tuning of its chemical reactivity can be achieved without serious perturbation in the reaction mechanism. In addition, the variation of adhesion energy depending on the kind of dopant originates from hybridization between the electronic states of the interface dopants (D_{TM}) and interface oxygen (O_i), *i.e.*, TM-ligand interaction, which can be described by traditional ligand field theory (LFT), despite the complexity, such as the symmetry of ligand field and the charge state of TM, compared to simple organometallic systems.

(2) Ordering of molecules with π-conjugated triangular core by switching hydrogen bonding and van der Waals interactions

Two-dimensional (2D) molecular networks on various surfaces are receiving much attention for the development of molecular electronic devices whose functionality is closely related to the spatial arrangement of molecules [Z. J. Donhauser et al., *Science* **292**, 2303 (2001)]. The 2D molecular network can also be used as a template to immobilize guest molecules containing specific functional groups in a well-ordered arrangement [J. A. Theobald et al., *Nature* **424**, 1029 (2003)].

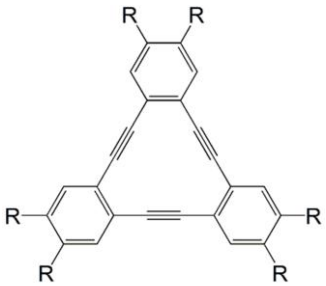

Figure 5. The chemical structures of alkoxylated derivatives of DBA.

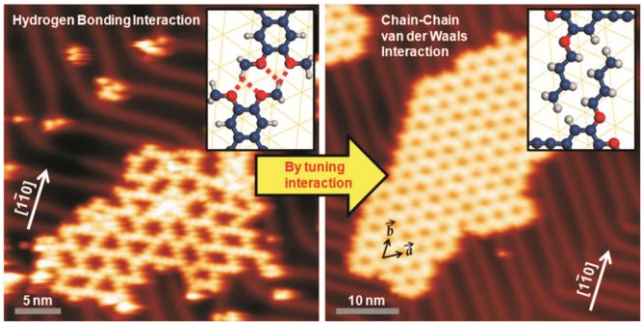

Figure 6. STM images of 2D molecular network formed by DBA-OC_1 (left, V_s = 2.0 V, I_t = 0.2 nA) and DBA-OC_4 (right, V_s = 2.0 V, I_t = 0.3 nA). Proposed models in insets describes hydrogen bonding and van der Waals interaction for the DBA-OC_1 (left) and DBA-OC_4 (right), respectively.

Through STM experiment, we observed that the homogeneity of the 2D molecular network of alkoxylated derivatives of triangular dehydrobenzo[12]annulene (DBA) (see Fig. 5) can be enhanced by changing the length of alkoxy group, from methoxy (DBA-OC_1) to butoxy (DBA-OC_4) as shown in Fig. 6.

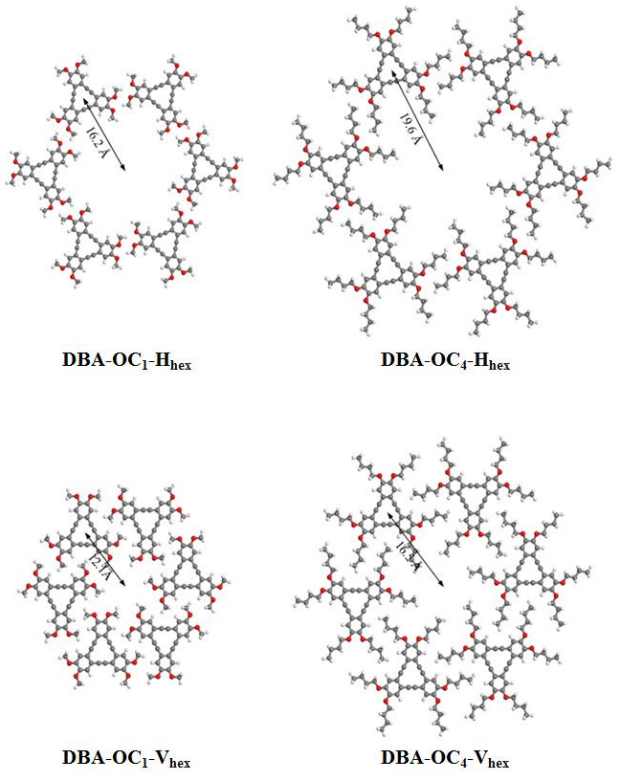

Figure 7. The optimized structures of two hexamers (H_{hex} and V_{hex}) composed of DBA-OC1 or DBA-OC4, as indicated. H_{hex} and V_{hex} denote the relative molecular orientations favorable for the hydrogen bonding interaction and the chain-chain vdW interaction, respectively.

DFT calculations were performed to investigate the experimental observations, which show that the nature of intermolecular interaction in the formation of molecular ordering changes from the hydrogen bonding interaction to the chain-chain van der Waals (vdW) interaction as the chain length of the peripheral alkoxy group increases. Based on the observed STM images (Fig. 6), we considered two six-fold hexamer structures composed of either DBA-OC_1 or DBA-OC_4, formed by hydrogen bonding and vdW interactions (designated H_{hex} and V_{hex}, respectively). Due to the large computational cost, we only considered the influence of molecule-molecule interaction on the formation of molecular ordering without counting molecule-substrate interaction. Figure 7 shows the optimized structures using the M06-2X hybrid functional and the 6-31G(d,p) basis set implemented

in the Gaussian 09 software package. It is known that the M06-2X functional provides particularly good performance in describing non-covalent interactions of main group elements. The structures of monomer and hexamer were optimized with D_{3h} and C_{6h} symmetries, respectively. The total electronic energies were evaluated by single-point energy calculations using the 6-311G(d,p) basis set.

Table 1. Binding energies (in kcal/mol) of two hexamers (H_{hex} and V_{hex}) composed of DBA-OC_1 or DBA-OC_4. The binding energy per molecule in each hexamer formation is shown in parentheses.

	H_{hex}	V_{hex}
DBA-OC_1	**43.5 (7.3)**	21.9 (3.7)
DBA-OC_4	25.0 (4.2)	**33.7 (5.6)**

Table 1 shows that the relative binding energies between two hexamer structures (i.e., H_{hex} and V_{hex}) dramatically change corresponding to the length of the alkoxy chain. Hydrogen bonding interactions between molecules are dominant in the formation of the DBA-OC_1 hexamer compared to vdW interactions. The binding energy of DBA-OC_1-H_{hex} (43.5 kcal/mol) is larger than that of DBA-OC_1-V_{hex} (21.9 kcal/mol), which implies that each DBA-OC_1 molecule in the DBA-OC_1-H_{hex} structure is energetically more stabilized by 3.6 kcal/mol compared to that in the DBA-OC_1-V_{hex} structure. The intermolecular C-H···O hydrogen bonding distances are in the range of 2.36 to 2.41 Å in the DBA-OC_1-H_{hex} structure. Contrarily, the DBA-OC_4-H_{hex} structure is less stable than the DBA-OC_4-V_{hex} structure by 8.7 kcal/mol. In the DBA-OC_4-H_{hex} structure, a decrease in the strength of hydrogen bonding interactions compared to the DBA-OC_1-H_{hex} structure is clarified by the extended distances between -O- and H-C- in the range of 2.91 ~ 3.22 Å. Our results clearly indicate that the longer alkoxy chain is unfavorable to hydrogen bonding formation due to enhanced steric hindrance, which prevents the mutual approach of two molecules closely enough to achieve the hydrogen bonding attraction. Accordingly, one DBA-OC_4 molecule in DBA-OC_4-V_{hex} can be more stabilized than that in DBA-OC_4-H_{hex} by 1.4 kcal/mol. Non-covalent interactions between neighboring molecules are further analyzed by the MULTIWFN software [T. Lu and F. Chen, *J. Comp. Chem.* **33,** 580 (2012)], as shown in Fig. 8.

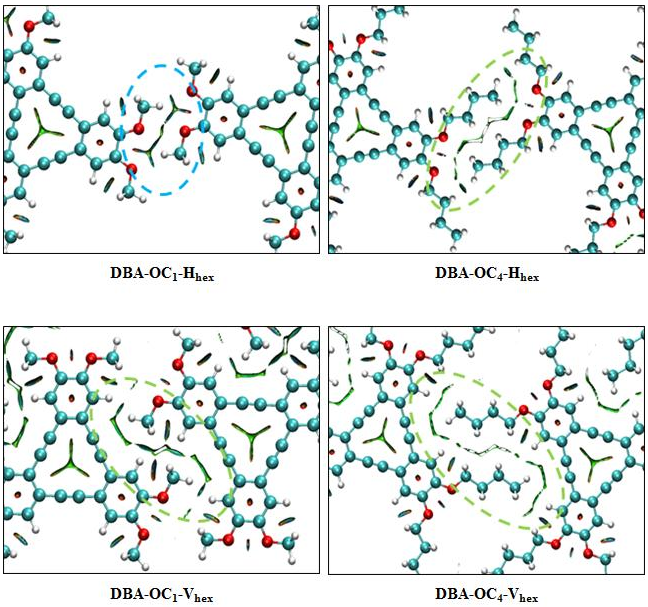

Figure 8. Gradient isosurfaces (s = 0.7 au) for two hexamers (H_{hex} and V_{hex}) composed of DBA-OC_1 or DBA-OC_4, as indicated. The surfaces are colored on a blue-green-red scale according to the values of sign(λ_2)ρ, ranging from -0.02 to +0.02 au. The primary intermolecular interactions are the C-H···O hydrogen bonding and the chain-chain vdW interaction, which are indicated by blue and green dotted circles.

The analyses for intermolecular interactions are based on the reduced density gradient ($s = 1/(2(3\pi^2)^{1/3}|\nabla\rho|/\rho^{4/3})$ which can be used to evaluate the deviation from a homogeneous electron distribution. In this methodology, stronger interactions than vdW interaction (e.g., attractive hydrogen bonding or repulsive steric effect) are also investigated using the sign of the Laplacian of the density, $\nabla^2\rho$ (see E. R. Johnson et al., *J. Am. Chem. Soc.* **132**, 6498 (2010) for the details of the theory). As shown in Fig. 8, the C-H···O hydrogen bonding (blue-colored region) plays a significant role only in

DBA-OC_1-H_{hex}. The other systems, however, show that vdW interactions (green-colored regions) are dominant between the alkoxylated DBA derivatives. Particularly, the morphological change in molecular ordering of DBA-OC_4 is well explained by the enlarged effective area of vdW interaction in DBA-OC_4-V_{hex} compared to DBA-OC_4-H_{hex}. Although the influence of substrate-molecule interaction is not encountered in the DFT calculations here, the calculation results show good agreement with the experimental results.

(3) Symmetry driven novel Kondo effect in FePc/Au(111)

The Kondo effect is one of the cooperative many-body phenomena in condensed matter physics. The spin degree of freedom of magnetic impurity is coupled with the conduction electrons at the Fermi sea of the reservoir, which causes the coherent spin-flip scattering between the impurity spin and conduction electrons. As a result, the magnetic moment of impurity spin is collectively screened through the formation of the many-body singlet state, Kondo resonance state, near the Fermi level below the Kondo temperature, T_K.

Not only the spin but also the other degrees of freedom can trigger the Kondo correlations [S. Sasaki et al., *Nature* **405**, 764 (2000).]. The orbital degree of freedom behaves as a pseudospin to bring about the Kondo effect through the many-body correlations to screen the pseudospin even in the absence of the real spin. Furthermore, in the presence of both orbital and spin degrees of freedom, the quantum fluctuations between these degrees of freedom give rise to the exotic Kondo effect obeying SU(4) symmetry. The orbital degeneracy commonly occurs in various organic molecules such as metal phthalocyanine, metal porphyrine and etc., and thus the SU(4) Kondo effect should be realized for these molecules by tuning the coupling between the molecules and the electron reservoir. Recent X-ray magnetic circular dichroism (XMCD) work of FePc on Au(111) has showed that the orbital degree of freedom survives and the molecule has sizable in-plane orbital magnetic moment [S. Stepanow et al., *Phys. Rev. B* **83**, 220401 (2011).]. Thus, we investigated the possibility of the SU(4) Kondo effect for FePc on Au(111) by ab-initio calculations based on DFT and NRG calculation together with STM and STS.

The geometric and electronic structures were investigated by DFT calculations with LDA+U. Consistent with the STM results, we found that the ontop and bridge species are stable [Fig. 9(a)]. Figure 9(b) shows the spin-polarized local density of states (SP-LDOS) projected on the d_{z^2} and d_π (d_{zx} and d_{yz}) orbitals of Fe for the ontop and bridge species. The valence of Fe can be approximately described as Fe^{2+} (S=1) with the electronic configuration of $(d_{xy})^2(d_{z^2})^1(d_{zx},d_{yz})^3$ similar to that of the isolated and bulk FePc. The splitting of d_{z^2} orbital reflects the stronger hybridization with the substrate than those of d_π orbitals. The overall LDOS features of both species are similar each other, but a marked difference is observed for the d_π orbitals. The peaks of d_{zx} and d_{yz} orbitals of the ontop species overlap each other whereas they are separate with 100 meV for the bridge species. The degeneracy in d_π orbitals in the isolated FePc survives for the ontop species while it is lifted for the bridge species.

The difference in the d_π orbitals of both species comes from the local symmetry of adsorption site. The differential charge distribution (DCD) and the differential local potential distribution (DLPD) clearly demonstrate the bonding nature and the symmetry, respectively. The cross section of DCD of the ontop species shows that the bond is formed mainly by the hybridization of d_{z^2} orbital with the Au atom beneath [Fig. 9(c)]. As a result, the 4-fold

symmetry is kept locally around the Fe atom as shown in the DLPD [Fig. 9(d)]. The holding of the 4-fold symmetry allows the degeneracy of d_{π} orbitals, resulting in the survival of the orbital degrees of freedom as reported by the XMCD work of FePc on Au(111). The bonding charges are distributed between the Fe atom and two nearest-neighboring Au atoms for the bridge species [Fig. 9(c)], reducing the local symmetry of ligand field to the 2-fold one as shown in Fig. 9(d).

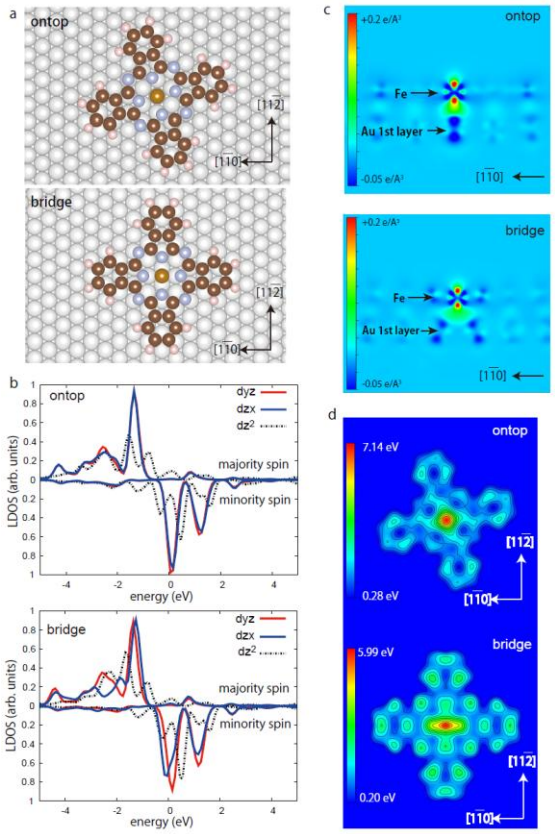

Figure 9. (a) The optimized structures of ontop and bridge FePc species on Au(111). (b) Spin-polarized local density of states (SP-LDOS) projected on the dzx, dyz and dz2 orbitals of Fe. The upper and lower panels show the SP-LDOS calculated for the ontop and bridge species, respectively. The dzx and dyz orbitals for the ontop species overlap each other. (c) The cross section of differential charge distribution (DCD) calculated for both species. (d) The differential local potential distribution (DLPD) calculated for both species. The figures a, c and d are rendered by VESTA [K. Momma and F. Izumi, *J. Appl. Crystallogr.* **41**, 653 (2008)].

The different electronic configuration of ontop species from the bridge species explains the site-specific spectral features observed by STS. Both ontop and bridge species have two unpaired electrons occupying in the d_{z^2} and d_{π} orbitals, which are coupled with the substrate electrons to cause the Kondo effect. The Kondo screening of two electrons proceeds in two stages for both species. Since the coupling strength of d_{z^2} with substrate is stronger than the d_{π}, the electron in the d_{z^2} is screened in the first stage, resulting in the broader peaks observed for both species. Subsequently, the electron localized in the d_{π} is screened in the second stage at lower temperature reflecting the smaller coupling of d_{π} with the substrate. The second-stage Kondo screening is observed for the ontop species as a sharp dip while it is not for the bridge species. The difference comes from the degeneracy of the d_{π} orbitals preserved only for the ontop species. Both spin and orbital degrees of freedom are available for the screening, i.e., the SU(4) Kondo channels open for the ontop species. In contrast, only the SU(2) channels are available for the bridge species due to the reduced symmetry. Compared to the SU(2) Kondo effect, the SU(4) Kondo temperature, $T_K^{SU(4)}$, is enhanced by the increase in the number of screening channels [J. S. Lim et al., *Phys. Rev. B* **74**, 205119 (2006)] so that the second-stage Kondo effect appears only for the ontop species. The second-stage Kondo signature cannot be observed for the bridge species because $T_K^{SU(2)}$ is much lower than $T_K^{SU(4)}$.

To quantitatively confirm this model, we calculated $T_K^{SU(4)}$ and $T_K^{SU(2)}$ by NRG based on the electronic structures derived from the LDA + U calculations. Increasing the energy separation between dzx and dyz orbitals (τ), the degeneracy is removed and then the crossover from the SU(4) to the SU(2) Kondo effect occurs. When $T_K^{SU(4)} = 2.7$ K, $T_K^{SU(2)}$ goes down to 0.2 K at $\tau = 100$ meV, which is merged into the background at the present experimental temperature (0.4 K). This supports the two-stage Kondo effect and the dependence of Kondo signature on the adsorption symmetry.

(4) New honeycomb lattice material - silicene on Ag(111)

Graphene, a single layer of sp2 bonded carbon atoms, has a honeycomb lattice with six-rotation symmetry. Because of its unique geometric symmetry, the electronic state of p_z orbital of carbon atom in graphene displays linear energy dispersion known as a Dirac cone. The characteristic linear dispersion around the Dirac cone suppresses the back-scattering of electron, which results in the high carrier mobility. Therefore, graphene is a promising material for next-generation devices.

Si is a member of the 14th group in the periodic table and takes the same valence electronic configuration as C so that Si shows various characteristics similar to those of C. Despite the similarities between C and Si, however, it has been considered that Si does not have an allotrope, which is the counterpart of graphene. Recently, the stability of the 2D honeycomb lattice of Si atoms, which is called silicene, has been investigated theoretically. DFT calculations show that a free-standing silicene is stable and the buckled silicene where the two Si atoms in the unit cell are vertically displaced in opposite directions is more stable than the planar one. Even this buckled structure different from planer graphene, the free-standing silicene possesses Dirac cone similar to graphene [S. Cahangirov et al., *Phys. Rev. Lett.* **102**, 236804 (2009)]. In addition, Si has stronger spin-orbit coupling than C, which is expected to induce spin-Hall effect and anomalous spin-Hall effect [M. Ezawa, *Phys. Rev. Lett.* **109**, 055502 (2012)].

To fabricate electronic devise, silicene is places on solid substrate and its electronic properties are perturbed by interfacial coupling. Very recently, silicene has been successfully synthesized on Ag(111) and ZrB_2 thin film by depositing Si atoms onto the substrates. In particular, the model structure and electronic properties in silicene on Ag(111) is still controversial. In this study, we investigate them by the combination of STM, LEED, and DFT.

First, we found two stable superstructures; one is 4×4 and the other is $(\sqrt{13}\times\sqrt{13})$R13.9°. In the 4×4 structure, the honeycomb lattice remains with six atoms displaced vertically, whereas the $(\sqrt{13}\times\sqrt{13})$R13.9° takes the regularly buckled honeycomb geometry. In the 4×4 silicene, previous angle-resolved photoelectron spectroscopy (ARPES) experiments showed a linear band dispersion, which was thought to be a signature of the Dirac fermions [P. Vogt et al., *Phys. Rev. Lett.* **108**, 155501 (2012)]. However, observing part of the linear band dispersion is not always sufficient as direct proof of the Dirac fermion, because part of a parabolic band can be well approximated as a linear band. Hence, judging from the ARPES data alone would cause errors in understanding its electronic character. The spectroscopic signatures of quantum Hall effect caused by the Landau quantization under a magnetic field provide solid evidence for the Dirac fermion. Thus measuring the current-voltage characteristics of the 4x4 silicene on Ag(111) under a magnetic field clarifies this puzzling contradiction. Experimentally, the Landau levels (LLs) are not appears in STS spectrum under magnetic field, which is the direct evidence that the electrons in the 4×4 silicene lose the characters of Dirac fermions.

This conclusion is reinforced by the DFT calculations. We considered vdW interactions between silicene and Ag(111), because the vdW interactions are important for understanding graphene on metal substrates. The results of band dispersion calculations with and without the vdW interactions are basically the same as shown in Fig. 10. The minor effect of vdW interaction in contrast to graphene on metals indicates the strong interaction between silicene and the underlying Ag(111) substrate. Although a plenty of electronic bands lie

around the Fermi level, they are not derived from the Si $3p_z$ orbitals. On the contrary, the bands derived from the Si $3p_z$ orbitals seem to be located below and above 1 eV from the Fermi level. Hence, the electronic states associated with Si are strongly hybridized with the substrate states. As a result, wave functions derived from the Si $3p_z$ orbitals are delocalized into the substrate. This reasonably explains the absence of LLs in the STS experiments.

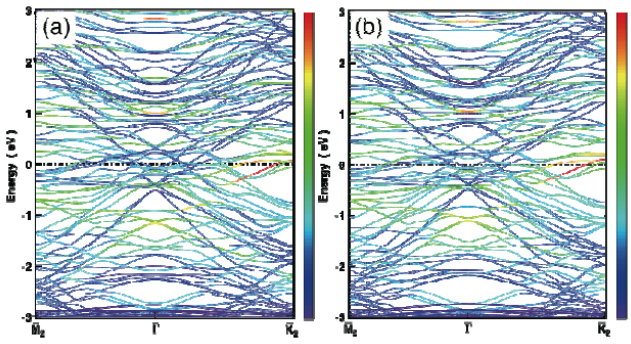

Figure 10. The calculated electronic band dispersion of the 4x4 silicene (a) without and (b) with including vdW interactions. The color bar shows the relative contribution of Si 3pz orbital to each band. The red and blue show the higher and lower contribution from Si 3pz orbital, respectively. The blue bands are basically derived from the substrate Ag.

4. Conclusion

We have tried to examine the molecular behaviors (i.e., chemical reaction, film formation, and Kondo effect) on the surface. First, we suggested the way to control the chemical reactivity of the ultrathin MgO film for the water dissociation by interface manipulation. Our systematic study on the doping of 3d TM into the oxide-metal interface provides a new perspective that the chemical reactivity of ultrathin oxide film grown on a metal substrate can be finely tuned by interface manipulation. The traditional LFT can be helpful to understand the variation of adhesion energy depending on the kind of dopant originates from hybridization between the electronic states of the interface dopants (D_{TM}) and interface oxygen (O_i), *i.e.*, TM-ligand interaction. Second, we revealed that the nature of intermolecular interaction in the formation of molecular ordering changes from the hydrogen bonding interaction to the chain-chain van der Waals (vdW) interaction as the chain length of the peripheral alkoxy group increases. Third, we found the possibilities of tailoring the quantum physical properties through the adsorption structure at surface. The important keyword is “symmetry”. As shown in FePc/Au(111), the orbital degeneracy in molecule is determined by the symmetry of local coordination on surface, which results in an emergence of a novel type of Kondo effect. Finally, in silicene monolayer on Ag(111), the breaking symmetry of honeycomb sublattice brings about the disappearance of Dirac fermions.

5. Schedule and prospect for the future

(1) Controlling chemical reactivity of ultrathin oxide film

Ultrathin oxide film grown on metal substrate has been a subject of great interest not only as a supporting material for chemically active nanoparticles but also as a catalyst in the field of heterogeneous catalysis, where it provides various ways to control the properties of adsorbates via following factors (See Fig. 11): (i) charge transfer between adsorbates and oxide-metal interface, which is closely correlated with the electronic affinity (EA) of adsorbate and workfunction reduction, (ii) adhesion between oxide and metal layers with strong polaronic distortion, (iii) film thickness, and (iv) the chemical composition of oxide surface.

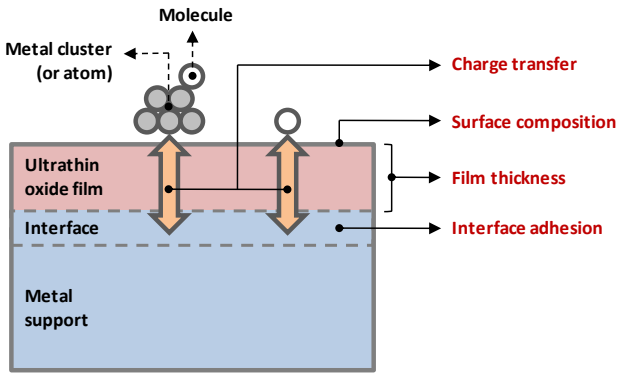

Figure 11. Schematic diagram for heterogeneous catalyst using ultrathin oxide film.

Therefore, we will continue our work to find the way for controlling the chemical reactivity using theoretical and experimental studies. In FY2013, we will extend our study into O_2 dissociation on MgO/Ag(100) with the interface dopants using combined STM and DFT methodology. In the case of O_2 dissociation on MgO/Ag(100), we should consider an influence from the charge redistribution between the oxide-metal interface and the adsorbate, because of O_2 has much higher EA than that of H_2O molecule. The other branch of our study is the clear understanding of the drawing effect at the oxide-metal interface, which can enhance the concentration of dopants at the interface. We believe that our study provides not only profound insight into the chemical reactivity control of ultrathin oxide film but also an impetus for investigating ultrathin oxide films for a wider range of applications.

(2) Molecular adsorption on solid surface: From single molecule to molecular network

We have recently examined a variety of molecular architectures on Au(111) using combined STM and DFT calculations. We studied an azobenzene derivative with two designed functional groups of different chain lengths to demonstrate a one-dimensional (1-D) molecular zipper. The formation and underlying mechanism of the molecular zipper resulted from combined hydrogen bonding and vdW interaction between adjacent molecules, investigated on the Au(111) surface. The influence of the balance between hydrogen bonding and vdW interactions on the formation of 2-D molecular network on the Au(111) was also investigated using alkoxylated derivatives of triangular dehydrobenzo[12]annulene (DBA) as building blocks. The relative importance of intermolecular hydrogen bonding versus vdW interactions depends on the length of the alkoxy groups. Such tunable intermolecular interactions balanced with surface–molecule interaction may eventually enable control of the formation of 2D molecular networks. In addition, a 2-D fluorinated fullerene ($C_{60}F_{36}$) superstructure was successfully fabricated on Au(111) in a well-ordered manner and investigated to reveal the driving force toward commensurate molecular film formation. The difference in the lowest unoccupied molecular orbital (LUMO) distribution among three isomers (C_3, C_1, and T) of $C_{60}F_{36}$ suggests that a well-ordered monolayer consists of only C_3 isomer, and the adsorption orientation is determined by localized distribution of its LUMO. Intermolecular C–F…π electrostatic interactions are other important factors in the formation of the superstructure.

Our results suggest that knowledge of molecule-molecule and molecule-substrate interactions and their balance, even on the noblest gold substrate, is of great importance to understand the formation mechanisms of various molecular architectures and further, to help determine the direction for efforts to design and control them for use in the future development of nano-structured molecular devices. In particular, we will continue the research for a variety of molecular assemblies on the surfaces as follows: (1) various π-conjugated molecules on solid surfaces and (2) the electronic structure of molecular wire on H-Si(100).

(3) Magnetism of molecules on various surfaces -combining DFT calculations and quantum many-body theories-

As series of studies have shown, depositing molecules on solid surfaces causes various effects such as charge transfer between molecules and surface which changes the electron states of molecules drastically. In addition, in order to discuss the magnetism in adsorbed molecules precisely, we need to treat many-body effects. This means that we have to construct a scheme which can treat the adsorption effects and many-body effect comprehensively. For this purpose, we try to combine the DFT calculations and quantum many-body theories. Specifically, we construct effective Hamiltonians based on DFT calculations results and solve them using quantum many-body theories. In FY2012, we found novel type Kondo effect can emerge in Fe-phthalocyanine (FePc) molecule at the ontop site of Au(111) from ab-initio calculations results and numerical renormalization group calculations. In FY2013, we further explore the Kondo effect in a single molecule on various metal surfaces and try to extend our simulation method.

Fiscal Year 2012 List of Publications Resulting from the Use of RICC

* The members registered as the user of RICC system in FY2012 are indicated by underline.

[Publication]

1. J. Jung, H.-J. Shin, Y. Kim, and M. Kawai, "Ligand field effect at oxide-metal interface on the chemical reactivity of ultrathin oxide film surface", *J. Am. Chem. Soc.*, **134**, 10554 (Jun. 2012).

2. E. Minamitani, N. Tsukahara, D. Matsunaka, Y. Kim, N. Takagi, and M. Kawai, "Symmetry-driven novel Kondo effect in a molecule", *Phys. Rev. Lett.* **109**, 086602 (Aug. 2012).

3. J.-H. Kim, K. Tahara, J. Jung, S. De Feyter, Y. Tobe, Y. Kim, and M. Kawai, "Ordering of molecules with π-conjugated triangular core by switching hydrogen bonding and van der Waals interactions", *J. Phys. Chem. C*, **116**, 17082 (Aug. 2012).

4. R. Arafune, H.-J. Shin, J. Jung, E. Minamitani, N. Takagi, Y. Kim, and M. Kawai, "Combined scanning tunneling microscopy and high-resolution electron energy loss spectroscopy study on the adsorption state of CO on Ag(001)", *Langmuir* **28**, 13249 (Sep. 2012).

5. C.-L. Lin, R. Arafune, K. Kawahara, M. Kanno, N. Tsukahara, E. Minamitani, Y. Kim, M. Kawai, and N. Takagi, "Substrate-induced symmetry breaking in silicene", *Phys. Rev. Lett.* **110**, 076801 (Feb. 2013).

[Oral presentation at an international symposium]

1. J. Jung, H.-J. Shin, Y. Kim, and M. Kawai, "Controlling chemical reactivity of ultrathin oxide film grown on metal substrate by interface manipulation", The 8th KIAS Electronic Structure Calculation Workshop, Korea Institute for Advanced Study (KIAS), Seoul, Korea (Jun. 2012). (Invited)

2. Y. Kim, From single molecule to molecular assembly: Making and manipulating interfaces, MIRC International Symposium on Molecular Architecture, Daejeon, Korea (Jun. 2012).

3. J. Jung, H.-J. Shin, Y. Kim, and M. Kawai, "Ligand field effect at oxide-metal interface on the chemical reactivity of ultrathin oxide film grown on metal substrate with interface dopants", The 16th International Conference on Solids Films and Surfaces (ICSFS-16), Genoa, Italy (Jul. 2012).

4. Y. Kim, J. Jung, H.-J. Shin, and M. Kawai, "Controlling reaction paths of a water molecule on an ultrathin MgO film with STM", The 16th International Conference on Solids Films and Surfaces (ICSFS-16), Genoa, Italy (Jul. 2012).

5. E. Minamitani, N. Tsukahara, D. Matsunaka, N. Takagi, M. Kawai, and Y. Kim, "The SU(4) Kondo effect in Fe-phthalocyanine molecules on Au(111)", The 2012 International Conference on Nanoscale + Technology (ICN+T2012), Paris, France (Jul. 2012).

6. N. Tsukahara, E. Minamitani, H. Terauchi, N. Takagi, Y. Kim, and M. Kawai, "Switching of Kondo resonance by molecular coordination: Iron phthalocyanine on Au(111)", The 2012 International Conference on Nanoscale + Technology (ICN+T2012), Paris, France (Jul. 2012).

7. E. Minamitani, N. Tsukahara, D. Matsunaka, N. Takagi, M. Kawai, and Y. Kim, "Symmetry driven exotic Kondo effect in a single molecule", The 14th International Conference on Vibrations at Surfaces (VAS-14), Kobe, Japan (Sep. 2012).

8. Y. Kim, “Mode-selective and state-selective chemistry of a single molecule on an ultrathin insulating film”, 2012 RCAS-TNNA Symposium - Recent Development in Nanomaterials: Structures, Dynamics & Applications, Taipei, Taiwan (Oct. 2012). (Invited)

9. Y. Kim, “Reaction control of a single molecule with STM”, Tsinghua-RIKEN Joint Workshop, Beijing, China (Oct. 2012). (Invited)

10. T. K. Shimizu, J. Jung, T. Otani, Y.-K. Han, M. Kawai, and Y. Kim, “Formation of 2D superstructure with wide bandgap n-type behavior”, American Vacuum Society (AVS) 59th International Symposium and Exhibition, Tampa, Florida, USA (Oct.-Nov. 2012).

11. J. Jung, H.-J. Shin, M. Kawai, and Y. Kim, “Single-molecule chemistry on an ultrathin insulating film”, 20th International Colloquium of Scanning Probe Microscopy (ICSPM20), Okinawa, Japan (Dec. 2012).

12. Y. Kim, “Single-molecule chemistry on un ultrathin MgO film”, Symposium on Surface and Nano Science 2013 (SSNS'13), Zao, Japan (Jan. 2013). (Invited)

13. Y. Kim, “From single molecule to molecular assembly: Fabricating, understanding and manipulating interfaces”, Korea-Japan Joint International Symposium on Molecular Systems (KJMS), Muju, Korea (Feb. 2013). (Invited)

14. T. K. Shimizu, J. Jung, and Y. Kim, “Combined STM and DFT study of 2D molecular superstructure formation on noble metals”, Korea-Japan Joint International Symposium on Molecular Systems (KJMS), Muju, Korea (Feb. 2013).

15. J. Jung, H.-J. Shin, M. Kawai, and Y. Kim, “Controlling chemical reactivity of ultrathin oxide film by interface manipulation”, Korea-Japan Joint International Symposium on Molecular Systems (KJMS), Muju, Korea (Feb. 2013).